UV Resonance Raman Study of β93-Modified Hemoglobin A: Chemical Modifier-Specific Effects and Added Influences of Attached Poly(ethylene glycol) Chains†

Laura J. Juszczak,‡ Belur Manjula,‡ Celia Bonaventura,§ Seetharama A. Acharya,‡ and Joel M. Friedman*,‡

Department of Physiology and Biophysics, Albert Einstein College of Medicine, 1300 Morris Park Avenue, Bronx, New York 10461, and Marine/Freshwater Biomedical Center, 135 Duke Marine Lab Road, Beaufort, North Carolina 28516-9721

Received June 12, 2001; Revised Manuscript Received October 12, 2001

ABSTRACT: The reactive sulfhydryl group on Cys β93 in human adult hemoglobin (HbA) has been the focus of many studies because of its importance both as a site for synthetic manipulation and as a possible binding site for nitric oxide (NO) in vivo. Despite the interest in this site and the known functional alterations associated with manipulation of this site, there is still considerable uncertainty as to the conformational basis for these effects. UV resonance Raman (UVRR) spectroscopy is used in this study to evaluate the conformational consequences of chemically modifying the Cys β93 sulfhydryl group of both the deoxy and CO-saturated derivatives of HbA using different maleimide and mixed disulfide reagents. Included among the maleimide reagents are NEM (*n*-ethylmaleimide) and several poly(ethylene glycol) (PEG)-linked maleimides. The PEG-based reagents include both different sizes of PEG chains (PEG2000, -5000, and -20000) and different linkers between the PEG and the maleimide. Thus, the effect on the conformation of both linker chemistry and PEG size is evaluated. The spectroscopic results reveal minimal perturbation of the global structure of deoxyHbA for the mixed disulfide modification. In contrast, maleimide-based modifications of HbA perturb the deoxy T state of HbA by "loosening" the contacts associated with the switch region of the T state $\alpha_1\beta_2$ interface but do not modify the hinge region of this interface. When the NEM-modified HbA is also subjected to enzymatic treatment to remove the C-terminal Arg α141 (yielding NESdes-ArgHb), the resulting deoxy derivative exhibits the spectroscopic features associated with a deoxy R state species. All of the CO-saturated derivatives exhibit spectra that are characteristic of the fully liganded R structure. The deoxy and CO derivatives of HbA that have been decorated on the surface with large PEG chains linked to the maleimide-modified sulfhydryl through a short linker group all show a general intensity enhancement of the tyrosine and tryptophan bands in the UVRR spectrum. It is proposed that this effect arises from the osmotic impact of a large, close PEG molecule enveloping the surface of the protein.

Hemoglobin (Hb)[1] functions as the primary oxygen transport protein in nearly all vertebrate organisms (*1*, *2*). More recently, other functions have been either identified or proposed for both vertebrate and nonvertebrate Hbs. Some of these additional functionalities are based on the presence of reactive sulfhydryl groups. The only reactive sulfhydryl groups in the Hb tetramer are those associated with Cys β93, and they have been implicated in a number of reactions that have important functional consequences for human adult hemoglobin (HbA). Formation of an *S*-nitrosothiol (SNO) derivative at β93 occurs to a limited extent in vivo and has been proposed (*3*, *4*) to play an important role in controlling vasoactivity. Direct evidence from spin resonance measurements suggests that β93 may also function as a deactivator of superoxide generated upon oxygen dissociation within the distal heme pocket (*5*). Furthermore, β93 modifications are being explored as a means of generating suitable candidates for clinically viable acellular oxygen transport reagents, such as HbA cross-linked between the two β93 residues using a PEG2000-based cross-linker [$(PEG2000)_2$XLHbA] (*6*) and antisickling forms of HbS, such as glutathionyl HbS (*7*, *8*).

Cys β93 is situated in a conformationally plastic domain containing residues whose interactions are directly linked to allosteric properties of the Hb tetramer (*9*−*11*). The reactivity of the β93 sulfhydryl is highly sensitive to both the quaternary and tertiary conformation of HbA (*12*−*21*). It has been proposed that in vivo functional roles of β93 are also modulated by the overall protein structure (*3*). Conversely, modification of the β93 sulfhydryl has been shown to have

† This work was supported in part by the National Institutes of Health through Grants R01 HL58247, R01 HL58248, R01 HL65188, and GM58890 and by the W. M. Keck Foundation.

* To whom correspondence should be addressed. Phone: (718) 430-3591. Fax: (718) 430-8819. E-mail: jfriedma@aecom.yu.edu.

‡ Albert Einstein College of Medicine.

§ Marine/Freshwater Biomedical Center.

[1] Abbreviations: HbA, human adult hemoglobin; XLHb, cross-linked hemoglobin; IHP, inositol hexaphosphate; GSH, glutathione; NEM, *N*-ethylmaleimide; NES, *N*-ethylsuccinimide; NO, nitric oxide; CO, carbon monoxide; PEG, poly(ethylene glycol); UVRR, ultraviolet resonance Raman; PBS, physiologic buffered saline; CPB, carboxypeptidase B; fwhm, full width at half-maximum.

10.1021/bi011212r CCC: $22.00
Published on Web 12/08/2001

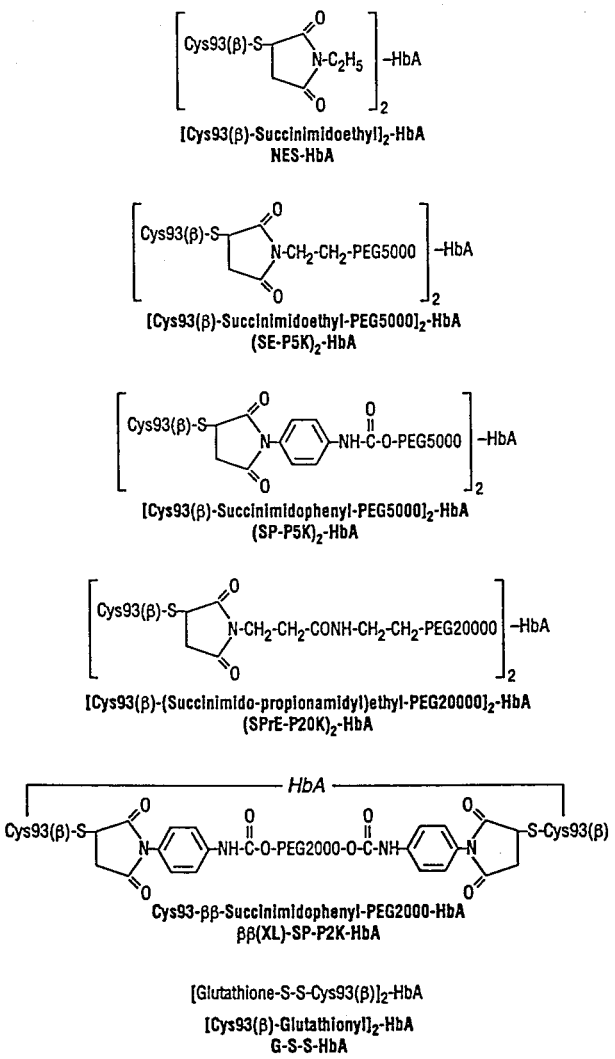

FIGURE 1: Schematic showing the structures and names of representative chemically modified Cys β93.

an impact on both the allosteric properties of HbA and the ligand binding reactivity of HbA within a given quaternary state (*21*−*25*). Little is known regarding the molecular details of how the binding of reagents to β93 impacts Hb structure.

In the study presented here, the tertiary conformation and the quaternary conformation of the globin are probed as a function of local perturbations of β93. Several of the derivatives are generated through a maleimide reaction with the sulfhydryl, resulting in a relatively large and rigid succinimidyl group attached to β93. A schematic showing the structure of many of the reagents used in this study is shown in Figure 1. Within this group of hemoglobins are different substituents covalently attached to the succinimidyl group, ranging from small ethyl groups such as *N*-ethyl succinimidyl HbA (NESHbA) to large poly(ethylene glycol) (PEG) chains connected to the succinimidyl group through either phenyl carbamyl, ethyl, or propionamidylethyl linkers. The impact of PEG size (2000, 5000, and 20000) and number (additional PEG chains covalently attached to thiopropyl-modified ϵ-amino groups) is also examined. For comparison purposes, we also probe a hemoglobin in which β93 is modified not with a maleimide reagent but via a disulfide linkage to glutathione (GSH). Also included in the study is the NES-modified HbA with an additional alteration arising from the enzymatic removal of the C-terminal arginine of the α-chains (Arg α141). On the basis of both spectroscopic and functional properties (high oxygen affinity and no cooperativity), this derivative, termed NESdes-ArgHbA, appears to be a suitable model for a species that remains in the R state even in the absence of a heme ligand (*21*, *22*, *26*).

The objective of this study is to use UV resonance Raman (UVRR) spectroscopy (*27*−*29*) as a probe of quaternary and tertiary structure to better understand the conformational consequences resulting both from chemical modification of the β93 sulfhydryl group and from the molecular groups such as PEG that are being covalently attached to the chemically modified sulfhydryl. The UVRR spectrum from hemoglobin has been shown to contain many tyrosine and tryptophan bands that change in intensity or peak position when structure changes in any one of several functionally important globin domains (*30*−*34*). In particular and most significant, spectral features reflect the determinants of the quaternary state, specifically in the "hinge" (Trp β37) and "switch" (Tyr α42) regions of the $\alpha_1\beta_2$ interface. There are also aspects of the spectra that respond to the packing of the A helix against the E helix, a feature that is indicative of different tertiary structures within a given quaternary state. In addition, the overall intensity pattern of many of the UVRR bands, relative to that of unmodified COHbA or deoxyHbA, can be used as an indication of the compactness of the R or T state tetramer (*31*, *33*, *35*−*40*). The study presented here utilizes many of these "reporters" of conformation to help not only evaluate the quaternary state status (R or T) of the different β93-modified hemoglobins but also explore conformational plasticity within quaternary states.

EXPERIMENTAL PROCEDURES

Hemoglobins Used in This Study

Eight different maleimide-modified Hbs were prepared. For two of the materials, NESHbA and NESdes-ArgHbA, *N*-ethylmaleimide (NEM) was used as the reactant. The added des-Arg α141 modification (NESdes-ArgHbA) was introduced to generate a noncooperative high-affinity species. For the other six Hbs, the following PEG-linked maleimides were used: (1) bis-maleidophenyl-carbamyl-PEG2000 (Bis-Mal-PEG2000), (2) maleidophenyl carbamyl(*O*′-methyl)-PEG5000 (Mal-Phe-PEG5000), (3) *O*′-(2-maleimidoethyl)-*O*′-methyl-PEG5000 (Mal-Eth-PEG5000), and (4) *O*-[2-(3-maleimidopropionamidyl)ethyl]-*O*′-methyl-PEG20000 (Mal-PEG20000). The third PEG-linked maleimide differs from the first two in that the resulting hemoglobin contains a succinimidoethyl linker between Cys 93 and the methoxy at the start of the PEG chain, whereas for the first two reagents, the linker is a phenyl carbamyl group. The fourth PEG reagent yields a species with a propionamidylethyl linker between the succinimidyl group and the methoxy at the origin of the PEG chain. The single non-maleimide-modified β93 species has a glutathione covalently attached to β93 through a disulfide linkage. Schematic drawings of several of the resulting modified β93 molecular species are shown in Figure 1. The preparative details for the modified Hbs mentioned above are described below.

Preparation of Hbs

HbA was purified from erythrocyte lysate, as described previously (*41*).

Cys 93ββ-Succinimidophenyl-PEG2000 HbA (ββ-SP-P2K-HbA). ββ-SP-P2K-HbA, a cross-linked (XL) derivative containing a single bifunctional PEG2000 chain bridging the two β93 residues, was prepared by reaction of HbA with Bis-Mal-Phe-PEG2000 in PBS (pH 7.4) followed by ion exchange chromatography on a CM-cellulose column, as described by Manjula et al. (*6*).

(Cys 93β-Succinimidophenyl-PEG5000)$_2$-HbA [(SP-P5K)$_2$-HbA] and (Cys 93β-Succinimidoethyl-PEG5000)$_2$-HbA [(SE-P5K)$_2$-HbA]. HbA was decorated on the surface at its Cys β93 residue with PEG5000 using two different PEG-maleimide reagents that differ in the spacer linking the reactive maleimide moiety to the PEG moiety (S. A. Acharya, unpublished results). (SP-P5K)$_2$-HbA was prepared by reaction of HbA with maleidophenyl carbamyl(*o*′-methyl)-PEG5000 (Mal-Phe-PEG5000) (BioAffinity Systems, Rockford, IL). Briefly, HbA (0.5 mM in tetramer) in PBS (pH 7.4) was reacted with a 5-fold molar excess of Mal-Phe-PEG5000 for 16−24 h in the cold. The modified protein was separated from the excess reagents by passing the reaction mixture through a Sephadex G25 column. (SE-P5K)$_2$-HbA was prepared by reaction of HbA with *O*-(2-maleimidoethyl)-*O*′-methyl-PEG5000 (Mal-Eth-PEG5000) (Fluka Biochemicals, Milwaukee, WI) employing the same procedure described above for the preparation of (SP-P5K)$_2$-HbA.

(Cys 93β-Succinimidophenyl-PEG5000)$_{6-8}$-HbA [(SP-P5K)$_{6-8}$-HbA] and (Cys 93β-Succinimidoethyl-PEG5000)$_{6-8}$-HbA [(SE-P5K)$_{6-8}$-HbA]. HbA decorated on the surface with six to eight copies of PEG5000 was prepared using two different PEG-maleimide reagents that differed in the spacer linking the reactive maleimide moiety to the PEG moiety. New thiol groups were introduced on HbA by reaction with 2-iminothiolane hydrochloride, which were subsequently reacted with the PEG5000 maleimide reagents. (SP-PEG5000)$_{6-8}$-HbA or (SP-PEG5000)$_{6-8}$-HbA was prepared by reaction of HbA with maleidophenyl carbamyl-*O*′-methoxy-PEG5000 or Mal-Phe-PEG5000 (BioAffinity Systems) in the presence of iminothiolane. Briefly, HbA (0.5 mM in tetramer) in PBS (pH 7.4) was incubated with 10 mM iminothiolane and 10 mM Mal-Phe-PEG5000 for 24 h at 4 °C, and the protein was separated from the excess reagents by gel filtration through a Sephadex G25 column in PBS (pH 7.4). (SE-PEG5000)$_{6-8}$-HbA or (SE-P5K)$_{6-8}$-HbA was prepared by the same procedure by reacting HbA with *O*-(2-maleimidoethyl)-*O*′-methyl-PEG5000 (Fluka Biochemicals) in the presence of iminothiolane. Size exclusion chromatography analysis on a Superose 12 column revealed the absence of unreacted HbA in both preparations, and in each case, the modified protein eluted as a single narrow band. An estimation of the number of sulfhydryl groups of the products generated by reaction of HbA with iminothiolane with and without the maleimide indicated that this procedure introduces six to eight PEG moieties per Hb tetramer. It should be noted that in the Results and Discussion below, these materials will be said to have six PEG chains attached despite the uncertainty in the actual number of PEG chains mentioned above.

(Cys 93β-Succinimidopropionamidylethyl-PEG20000]$_2$-HbA [(SPrE-P20K)$_2$-HbA]. (SPrE-P20K)$_2$-HbA was prepared by reaction of HbA with methoxy poly(ethylene glycol) maleimide 20000 {*O*-[2-(3-maleimidopropionamidyl)ethyl]-*O*′-methyl-PEG20000} (Shearwater Polymers, Inc., Huntsville, AL). Briefly, HbA (0.5 mM in tetramer) in PBS (pH 7.4) was reacted with a 5-fold molar excess of the methoxy-PEG20000 reagent for 24 h at 4 °C. The reaction mixture was desalted through a Sephadex G25 column, ultrafiltered through an Amicon Centriprep 100K concentrator (Amicon Inc., Beverly, MA), and further purified on a preparative (2.6 cm × 130 cm) Superose 12 column in PBS (pH 7.4).

(Cys 93β-Glutathionyl)$_2$-HbA (GSSHbA). GSSHbA was prepared by a two-step process. In the first step, HbA was converted to a mixed disulfide of thiopyridine. HbA (1 mM in heme) in PBS (pH 7.4) was incubated with a 5-fold molar excess of dithiopyridine on ice for 1 h. The thiopyridyl HbA was separated from the excess reagents by gel filtration through a column of Sephadex G25 in PBS (pH 7.4). The thiopyridyl HbA (0.5 mM in heme) was then incubated with a 20-fold molar excess of reduced glutathione at 4 °C overnight and gel filtered on Sephadex G25 again to isolate the glutathione−HbA adduct. Modification of Cys β93 was confirmed by the failure of GSSHbA to react with Mal-Phe-PEG5000, and by the absence of any free thiols in oxy-GSSHbA on titration with 4,4-dithiopyridine by the method of Ampulski et al. (*42*). Isoelectric focusing analysis demonstrated that the product was homogeneous and free of unreacted HbA.

(Cys 93β-Succinimidoethyl)$_2$-HbA (NESHbA). NESHbA was made by treating 3 mL of a 0.05 M Bis-Tris, 1 mM (heme) HbA solution with 3 mM NEM achieved by adding 45 μL of 0.2 M NEM (protein:NEM ratio of 1:3). The reaction mixture was incubated at 5 °C for 1 h. The reaction was stopped by dialysis against 0.05 M Hepes at pH 7.4 overnight.

NESdes-ArgHbA. The des-Arg(α141)HbA was prepared using carboxypeptidase B (CPB) digestion. A 1 mL sample of HbA was passed down a Pharmacia type PD-10 column and eluted with 0.05 M Tris buffer (pH 8.3). The Hb concentration was approximately 1 mM in heme. An aliquot of 0.5 mL of a CPB stock solution (7.6 mg/mL) was then added to 4.4 mL of the eluted Hb solution (77 mg of heme), yielding a 1:200 protein:enzyme ratio. Prior to the addition of the CPB, 45 μL of 100 mM carboxypeptidase A inhibitor was added to the eluted HbA stock solution, yielding a concentration of 1 mM. After the addition of CPB, the sample was converted to the CO form and incubated at 37 °C for 1 h, followed by dialysis against 0.05 M Bis-Tris buffer (pH 7.4). The resulting des-ArgHbA was then modified with NEM as described above for the preparation of NESHbA.

UV Resonance Raman Spectroscopy

The 229 nm-excited, continuous wave, UV resonance Raman (UVRR) spectra of solution phase deoxy and CO derivatives of β93-modified HbA were generated using a previously described apparatus (*43*). The cooled (∼4−10 °C), sample-containing NMR tubes were spun and rastered vertically to minimize sample heating and laser-induced degradation. The incident laser power was 1.8 mW. Typi-

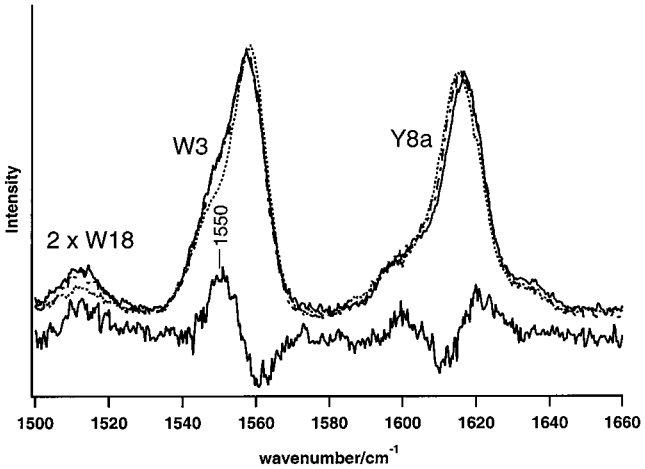

FIGURE 2: High-frequency portion of the 229 nm-excited UVRR spectra of deoxyNESHb (−•−), deoxyHbA (—), and CONESHb (•••). Also shown is a blowup of the intensity-normalized Y8a bands (top) and the difference spectra (bottom): deoxyNESHb − CONESHb (—) and deoxyHbA − COHbA (- - -).

cally, four 3 min acquisitions were accumulated for each ligation state of each Hb variant. Absorption spectra were collected before and after exposure to the UV laser beam. If absorption changes were noted, the sequential UVRR acquisitions were examined for evidence of band changes. Acquisitions that exhibited changes were rejected and not included in the final averaging of the UVRR spectra. The spectral pixel width is 0.4 cm^{-1}/pixel. The experimental error in peak position is ± 0.3 cm^{-1}, as determined statistically from the changes in the 1609.2 cm^{-1} peak of the calibration standard, indene, the UVRR spectrum of which is collected each time data are acquired.

The probed solutions contained 0.2 M selenate that is used as an internal intensity standard. Unless otherwise stated, comparisons between spectra are normalized with respect to the internal intensity standard. All of the probed samples consisted of 0.5 mM Hb (heme concentration) in 50 mM Bis-Tris acetate buffer (pH 6.5).

Curve fits to W3 bands were carried out using the software program GRAMS/32 AI, version 6.00 (Galactic Industries Corp., Salem, NH).

RESULTS

Overview of UVRR Spectra. In solution, the binding of CO to deoxyHbA initiates an undetermined sequence of tertiary structure changes that ultimately result in a quaternary switch from the low-affinity T structure to the high-affinity R structure. In all but one figure (Figure 4) is the full UVRR spectrum (800−1680 cm^{-1}) truncated to 1500−1660 cm^{-1} because this region contains the bands that have been best characterized with respect to changes in the hemoglobin quaternary structure, i.e., W3, 2×W18, and Y8a.

The W3 band at ∼1558 cm^{-1} has two contributions (*30*, *31*, *34*, *38*). The central feature that peaks at ∼1558 cm^{-1} is derived from the two A helix tryptophans (α14 and β15), whereas the T−R sensitive shoulder at ∼1550 cm^{-1} originates from Trp β37. In 229 nm-generated UVRR spectra (*30*−*32*, *37*, *44*), the intensity of this β37-associated shoulder increases due to the increase in the extent of hydrogen bonding between Trp β37 and Asp α94 when switching from the R to the T state. It has been shown through a comparison

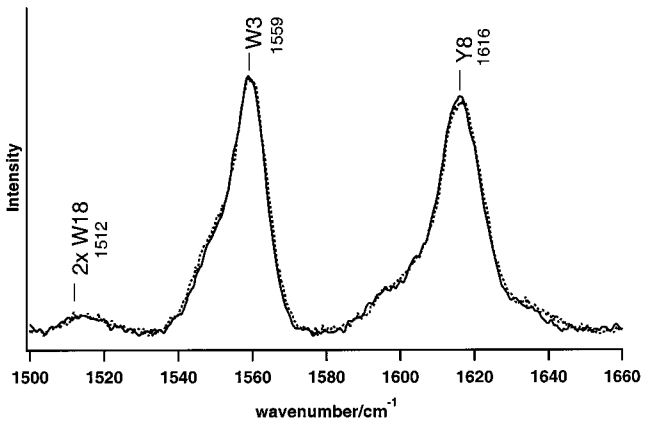

FIGURE 3: Comparison of the intensity-normalized UVRR spectra of COHbA (•••) and deoxyNES-desArgHb (—).

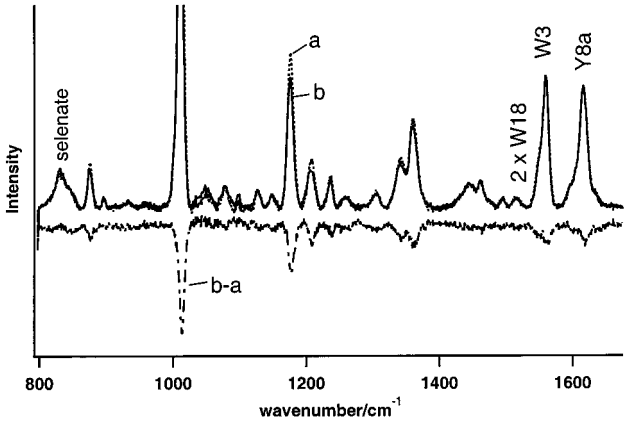

FIGURE 4: Comparison of the full UVRR spectra of COHbA [a (•••)] and deoxyNES-desArgHb [b (—)]. The UVRR difference spectrum, deoxyNES-desArgHb − COHbA, is also shown at the bottom.

of UVRR spectra for several crystalline, deuterated, and nondeuterated tryptophan derivatives with the crystal structures for those derivatives that the W3 band position correlates with the indole ring $C_\alpha-C_\beta$ dihedral angle (*45*, *46*).

The weak band at 1512 cm^{-1} has undergone several reassignments (*31*, *38*, *44*) but is now definitely attributed, first, to tryptophan (*47*) and, specifically, to the 2× overtone of the W18 mode (*48*). This band shows a decrease in intensity when HbA switches from the T state to the R state (*30*−*32*, *44*) that is attributed to Trp β37 in the hinge region of the $\alpha_1\beta_2$ interface on the basis of its behavior in the HbAβ37Trp → Glu mutant (*47*).

The tyrosine Y8a band at ∼1616 cm^{-1} exhibits an ∼1−2 cm^{-1} shift to higher frequency when liganded R state HbA is converted to the deoxy T state (*30*, *31*), resulting in a sigmoidal or derivative-shaped UVRR difference spectrum (Figure 2, bottom). This frequency shift originates primarily from Tyr α42 (*38*, *40*, *49*) in the hinge region of the $\alpha_1\beta_2$ interface.

Summary of Spectral Data Changes. Table 1 provides a summary of the spectral changes discussed below. The UVRR band data have been related to specific conformational degrees of freedom (*35*). The first column contains the shift in frequency for the Y8a band relative to the Y8a frequency for the CO derivative. For deoxyHbA, this frequency shift is ∼1.5 cm^{-1}. The second column shows the

Table 1: Species, Ligation State, and IHP-Dependent Spectral Changes in the 229 nm-Excited UVRR Spectra of Cys β93-Modified HbAs at pH 6.5[a]

		ΔY8a	$\Delta I_{Y8a}/I_0$	$\Delta I_{W3}/I_0$	$\Delta I_{W3(\beta37)}/I_{CO}$	$\Delta I_{2W18}/I_{CO}$
NESHb	CO	0.0	4.6	2.9	0.0	0.0
	deoxy	0.7	3.0	5.0	25.1	78.7
	deoxy + IHP	1.4				
NESdes-ArgHb	CO	0.0	1.5	−5.8	0.0	0.0
	deoxy	0.4	9.0	10.3	−28.6	1.8
GSSHb	CO	0.0	23.5	15.3	0.0	0.0
	deoxy	1.0	18.5	15.3	19.2	29.9
	deoxy + IHP	1.4	11.1	12.9	22.4	29.9
$\beta\beta$-P2K-Hb	CO	0.0	−2.1	−6.2	0.0	0.0
	deoxy	1.1	−2.1	−5.0	16.2	70.6
	deoxy + IHP	1.0	1.1	−5.0	27.1	96.1
$(SP\text{-}P5K)_2$-Hb	CO	0.0	0	3.8	0.0	0.0
	deoxy	1.0	−5.4	0	1.6	13.6
	deoxy + IHP	1.4	1.1	−5.1	35.3	79.7
$(SE\text{-}P5K)_2$-Hb	CO	0.0	−47.3	−53.8	0.0	0.0
	deoxy	1.1	−31.2	−27.9	26.6	130.5
$(SP\text{-}P5K)_6$-Hb	CO	0.0	−11.0	0	0.0	0.0
	deoxy	1.3	−11.0	0	12.8	37.0
$(SE\text{-}P5K)_6$-Hb	CO	0.0	−63.9	−88.9	0.0	0.0
	deoxy	1.6	−37.5	−46.9	−6.5	81.0
$(SPr\text{-}P20K)_2$-Hb	CO	0.0	−34.7	−17.3	0.0	0.0
	deoxy	1.7	−40.3	−32.1	3.80	137.5

[a] $\Delta Y8a = \nu_x - \nu_{CO}$, where ν is the frequency (± 0.3 cm^{-1}) of Y8a and x is the particular derivative for species in question and CO is the designation for the CO derivative for the Hb species in question. All values for the CO derivatives are thus zero. $\Delta I_{Y8a}/I_0 = (I_{COHbA} - I_x)/I_{COHbA}$ multiplied by 100, where I is the intensity of Y8a. $\Delta I_{W3}/I_0 = (I_{COHbA} - I_x)/I_{COHbA}$ multiplied by 100, where I is the intensity of the central peak of the W3 band. $\Delta I_{W3(\beta37)}/I_{CO} = (I_x - I_{CO})/I_{CO}$ multiplied by 100, where I_x is the intensity of the β37 shoulder of the W3 band for the species in question and I_{CO} is the intensity of the β37 shoulder of the W3 band for the corresponding CO derivative of the sample under examination. $\Delta I_{2W18}/I_{CO} = (I_x - I_{CO})/I_{CO}$ multiplied by 100, where I_x is the intensity of the 2×W18 band for the species in question and I_{CO} is the intensity of the 2×W18 band for the corresponding CO derivative of the sample under examination. In some instances, there was sufficient uncertainty in the normalization process to make it impractical to present the intensity changes with any degree of confidence. These values were omitted from the table.

percent intensity change of the Y8a band relative to that of COHbA. Enhancement of the intensity appears as a negative number. Similarly, the third column shows the percent intensity change for the W3 α14/β15 band. Again, negative values indicate an increase in intensity. The fourth column lists the percent intensity change of the Trp β37 shoulder of the W3 band. The values that are presented are referenced against the CO derivative of the sample in question, and an increase in intensity is here a positive number. Because of the inherent difficulty in obtaining unique curve fits to the W3 bands, intensities for the deconvoluted Trp β37 bands of W3 have an estimated uncertainty of several percent. The reported (*35*) reduced W3 band β37 intensity change [$(I_{deoxyHb} - I_{COHb})/I_{COHb}$] for HbA is 37%. The corresponding W3/β37 reduced intensity change calculated from the deoxyHbA UVRR spectrum shown in Figure 2 and the COHbA UVRR spectrum given in Figure 3 is 39%. The intensity change for the 2×W18 band in column 5 of Table 1 is similarly calculated. Large values are associated with the most T-like structures. The weak intensity of this band for the liganded R state species introduces a large element of uncertainty into this parameter; nonetheless, it does allow for a comparison of derivatives for a given sample.

NESHbA. Figure 2 shows the high-frequency segment of the 229 nm-excited UVRR spectra from deoxyNESHbA, CONESHbA, and deoxyHbA. The deoxy − CO difference spectrum for NESHbA, shown in Figure 2 (bottom), exhibits many of the features observed for a similar HbA difference spectrum, which is superimposed (*38*). The latter is calculated from the deoxyHbA UVRR spectrum shown above in Figure 2 and the COHbA UVRR spectrum given in Figure 3. The 2×W18 band shows a comparable intensity enhancement in going from CONESHbA to deoxyNESHbA. The characteristic liganded R → deoxy-T enhancement of the W3 1550 cm^{-1} shoulder is clearly seen in the difference spectra as well as in a comparison of the separate spectra; its intensity is greater than that for the HbA difference. Additionally, a negative W3 band difference is centered at 1560 cm^{-1} but is not found in the UVRR difference spectrum for wild-type HbA (*38*). The derivative-shaped feature observed in the Y8a region of the deoxy − CO difference spectrum is similar in intensity and shape to that of HbA with a peak-to-peak reduced intensity [$\Delta I_{Y8a}/I_{Y8a}$(COHb)] of 0.36. The corresponding peak-to-peak Y8a reduced intensity for the HbA difference spectrum (Figure 2, bottom) is 0.39.

An expanded detail of the Y8a peaks in Figure 2 is also shown. The CONESHbA peak position is 1615 ± 0.3 cm^{-1}. It can be seen that the band for deoxyNESHbA is broadened compared to that of deoxyHbA. The high-frequency edge of the former overlaps that of deoxyHbA; however, its low-frequency edge extends much further toward that of the CO derivative. Thus, the Y8a band of deoxyNESHbA is almost as wide as the combined Y8a band for deoxyHbA and COHbA. The deoxyNESHbA spectrum does not respond significantly to the addition of IHP (data not shown).

NESdes-ArgHbA. Figure 3 shows the similarity in the W3 and Y8a peak positions between the intensity-normalized UVRR spectra of COHbA and deoxyNESdes-ArgHbA. When the spectra are normalized to the internal standard, the peak intensities for deoxyNESdes-Arg are reduced relative to those from COHbA, as seen in Figure 4. In contrast, both the peak frequencies and intensities in the spectra of COHbA and CONESdes-ArgHbA are essentially identical (data not shown). The peak-to-peak Y8a reduced

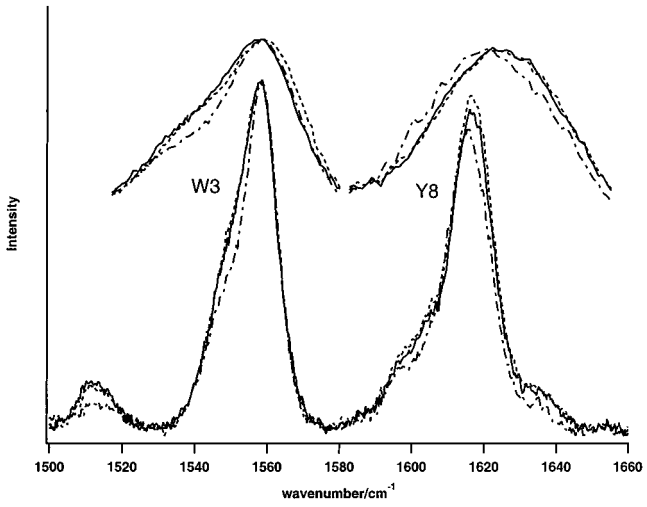

FIGURE 5: Comparison of the UVRR spectra of deoxyGSSHb (—), deoxyGSSHb with IHP (- - -), and COGSSHb (—•—) with blowups of the intensity-normalized W3 and Y8a bands.

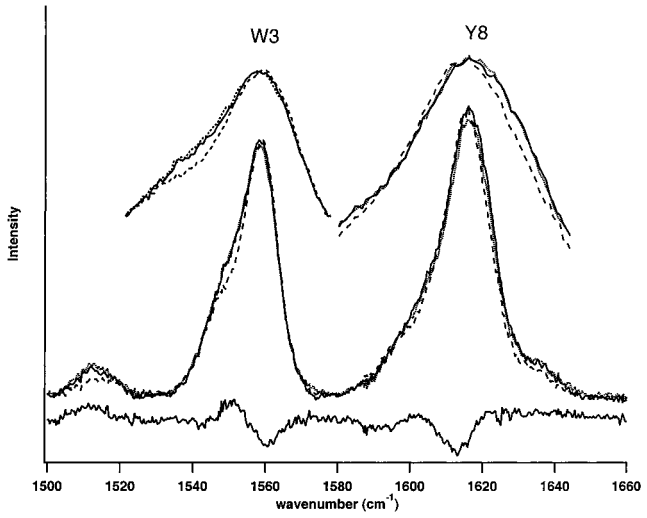

FIGURE 6: Comparison of the UVRR spectra of $\beta\beta$-SP-P2K-deoxyHb (—), $\beta\beta$-SP-P2K-deoxyHb with IHP (•••), and $\beta\beta$-SP-P2K-COHb (- - -) with blowups of the intensity-normalized W3 and Y8a bands. The difference spectrum, (deoxy − CO)$\beta\beta$-SP-P2K-HbA, is shown at the bottom.

intensity for the difference spectrum (deoxyNES-desArgHb − COHbA, Figure 4, bottom) is 0.17.

GSSHbA. Figure 5 compares the high-frequency region of the UVRR spectra from CO and deoxy ± IHP derivatives of GSSHbA. This modified hemoglobin exhibits the standard deoxy T versus liganded R differences in the 2×W18 band (intensity change), the W3 band (intensity change in the 1555 cm^{-1} shoulder), and the Y8a band (frequency shift). It can also be seen that the addition of IHP to the deoxy derivative has very little impact on most of the spectral features; however, it does cause an additional increase in the frequency of Y8a and increases the relative intensity of Y8a. It also appears that addition of IHP shifts the central W3 peak to a higher frequency.

$\beta\beta$-SP-P2K-HbA. Figure 6 shows the high-frequency region of the UVRR spectra of the CO and deoxy ± IHP derivatives of PEG2000-cross-linked Hb. The figure shows the deoxy-T state versus CO − R state differences in the 2×W18, W3, and Y8a (Y8a peak-to-peak reduced intensity *I* of 0.16) bands. As for the deoxyNESHbA results (Figure 2), a broadening in the Y8a band of the deoxy derivative (Figure 6, right inset) occurs. Analogously, a negative W3 band difference is located at 1560 cm^{-1}.

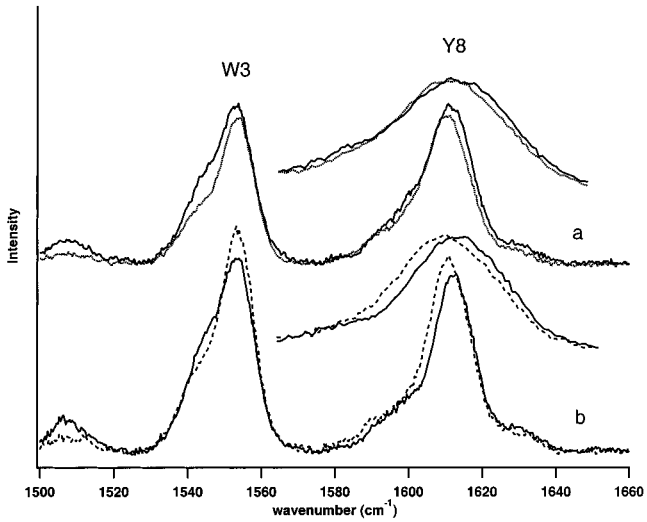

FIGURE 7: Deoxy vs CO comparison of the UVRR spectra for two different $(P5K)_2$-Hb samples. The spectra in panels a and b are representative of $(SP\text{-}P5K)_2$-Hb and $(SE\text{-}P5K)_2$-Hb, respectively. For both panels, the spectra of the deoxy derivative are the solid lines whereas the dotted or dashed lines represent the spectra of the CO derivatives.

$(SP\text{-}P5K)_2$-Hb and $(SE\text{-}P5K)_2$-Hb. Figure 7 shows the high-frequency region of the UVRR spectra of the deoxy and CO derivatives of the two different PEG5000 β93-modified HbAs described in Experimental Procedures. The phenyl carbamyl-linked $(SP\text{-}P5K)_2$-Hb results are shown in Figure 7a, whereas the ethyl-linked $(SE\text{-}P5K)_2$-Hb results are given in Figure 7b. In both cases, spectral signatures of the deoxy-T and liganded R states are apparent in the 2×W18 (1512 cm^{-1}), W3, and Y8a bands. There are, however, differences from the pattern seen for HbA. The intensities of the W3 and Y8a bands of the CO derivative versus the deoxy derivative are essentially the same (<10% difference; see Table 1) for the phenyl carbamyl-linked Hb (Figure 7a), whereas for the ethyl-linked Hb (Figure 7b), the corresponding band intensities are significantly higher for the CO derivative (Table 1). The Y8a band detail reveals that although the band positions for the CO and deoxy derivatives are similar for the two derivatives, the band for deoxy$(SP\text{-}P5K)_2$-Hb is broader (fwhm = 16.3 cm^{-1}) than that for deoxy$(SE\text{-}P5K)_2$-Hb (fwhm = 13.5 cm^{-1}). It can be seen in the expanded Y8a insets that the low-frequency edge of the Y8a band for the phenyl carbamyl-linked deoxy derivative overlaps that of the CO derivative, whereas for the ethyl-linked derivative, there is a clear separation of two bands (deoxy and CO) of comparable width.

A significant difference between the spectra of the two differently linked $(P5K)_2$-Hb samples is apparent when comparing the intensity of spectral bands to those from HbA (Table 1). The spectra for $(SP\text{-}5PK)_2$-Hb exhibit a minimal intensity difference, whereas those for $(SE\text{-}P5K)_2$-Hb exhibit a substantial enhancement of the W3 and Y8a bands for both deoxy and CO derivatives.

$(SP\text{-}P5K)_6$-Hb and $(SE\text{-}P5K)_6$-Hb. The phenyl carbamyl- and ethyl-linked pegalated Hbs discussed above were further decorated on the surface with four additional (possibly six; see Experimental Procedures) PEG5000 chains. Figure 8

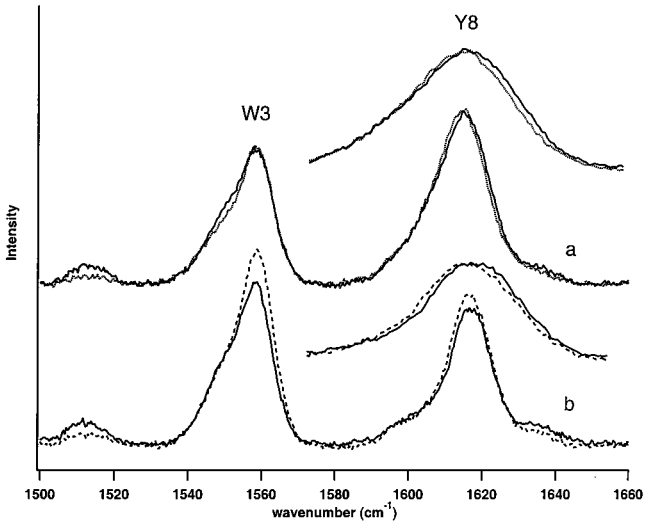

FIGURE 8: Deoxy vs CO comparison of the UVRR spectra of two different $(P5K)_6$-Hb samples. The spectra in panels a and b are representative of $(SP\text{-}P5K)_6$-Hb and $(SE\text{-}P5K)_6$-Hb, respectively. For both panels, the spectra of the deoxy derivative are the solid lines whereas the dotted or dashed lines represent the spectra of the CO derivatives.

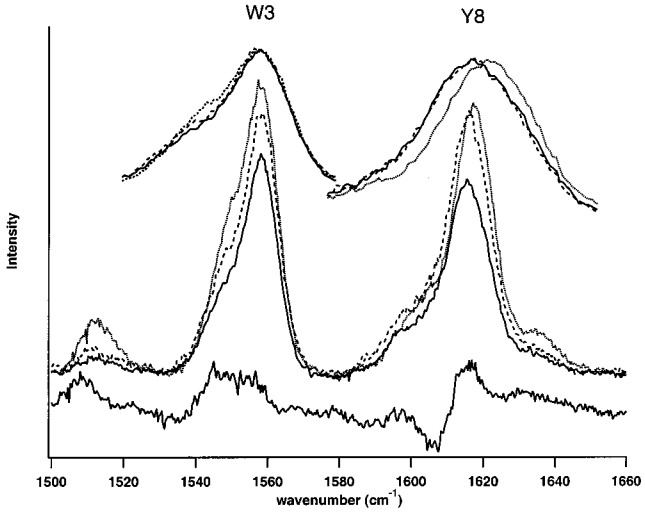

FIGURE 9: Comparison of the UVRR spectra of $(SPr\text{-}P20K)_2$-deoxyHb (•••), $(SPr\text{-}P20K)_2$-COHb (- - -), and COHbA (—) with blowups of the intensity-normalized W3 and Y8a bands. The difference spectrum, $(SPr\text{-}P20K)_2$-deoxyHb − $(SPr\text{-}P20K)_2$-COHb, is also shown at the bottom.

shows the high-frequency region of the UVRR spectra of the deoxy and CO derivatives of these species. The spectral patterns associated with the 2×W18 (1512 cm^{-1}), W3, and Y8a bands are similar to those observed for the $(P5K)_2$-Hb samples. The intensity pattern relative to HbA is also similar to what is observed for the Hb $5K_2$ samples, with the ethyl-linked $(P5K)_6$ samples displaying a general intensity enhancement of both tyrosine and tryptophan bands (Table 1). UVRR results on a neat solution of the phenyl PEG linker at the same concentration that was used for $(SP\text{-}P5K)_6$-Hb (data not shown) revealed that the weak signal centered at ∼1616 cm^{-1} accounts for the 11% increase in Y8a intensity for $(SP\text{-}P5K)_6$-Hb relative to COHbA (Table 1). The difference in signal enhancement between the phenyl- and ethyl-linked Hbs cannot be attributed to self-absorption by the phenyl groups because the laser is configured for front surface scattering off the sample.

$(SPr\text{-}P20K)_2$-Hb. Figure 9 shows the high-frequency region of the UVRR spectra from COHbA, $(SPr\text{-}P20K)_2$-COHbA, and $(SPr\text{-}P20K)_2$-deoxyHb. As with the other surface-decorated Hbs [$(P5K)_2$ and $(P5K)_6$] having non-phenyl-based PEG linkers, the intensity of the W3 and Y8a bands is enhanced relative to that of HbA (Table 1). The standard deoxy versus CO spectral differences are also still apparent in this sample (Figure 9, bottom), and the Y8a peak-to-peak reduced intensity for the difference spectrum is comparable in magnitude, 0.32. It is to be noted that this Y8a spectral difference is without the broadening seen in the results for the deoxy derivatives of the other maleimide-modified samples discussed above.

DISCUSSION

UVRR as a Probe of Hemoglobin Structure. The absence of a W3 difference peak (1560 cm^{-1}) for the HbA α14/β15 Trps (Figure 2, bottom) shows that the two A helix tryptophans and their environment are unchanged at the R and T state end points in wild-type HbA (*30*, *31*). Both α14 and β15 are hydrogen bonded to residues on the E helix, and changes in the packing of the A and E helices likely impact this hydrogen bonding pattern (*37*), resulting in intensity changes in the central peak of the W3 band as seen in Figures 2, 4, and 6−9. Studies on the partially unfolded and refolded COMb in porous sol−gel matrices suggest that changes (either static or dynamic) in the exposure of the A helix tryptophan to solvent can also be contributing to these intensity effects (*47*). In either case, a decrease in the intensity of the W3 band is likely associated with looser packing (greater separation) of the A and E helices.

The Y8a derivative-shaped, deoxyHbA-COHbA UVRR difference band originates largely from T to R changes associated with the interfacial Tyr α42 and the accompanying loss of its hydrogen bond to Asp β99 (*14*−*18*). On the basis of the UVRR spectra from the mutant hemoglobin Hb(α140 Tyr → His), the 2 cm^{-1} Y8a shift has also been attributed to changes associated with the C-terminal, penultimate Tyr α140 (*49*). This conclusion has been questioned (*50*), and the absence of any deoxy → CO shift in the Y8a band from the fully cooperative mutant Hb(α42 Tyr → Ala) (L. J. Juszczak and J. M. Friedman, unpublished results) suggests that the contribution to the Y8a shift from Tyr α140 may be specific to that particular mutant and not applicable to other hemoglobins.

On the other hand, intensity changes in Y8a, without frequency shifts, have been linked to variations in the packing of the penultimate tyrosines (α140 and β145) that alter either hydrogen bonding to the carbonyl of the respective FG5 valines or exposure to solvent (*35*, *50*−*53*). It has been argued that the hydrogen bond between the penultimate tyrosines and the FG5 valines is an important component in the scaffolding that maintains the spatial separation between globin helices. Within this well-supported model, changes in the scaffolding that result in a tighter packing of helices are reflected in a general increase in the relative intensity of many of the 229 nm-excited UVRR bands, whereas looser packing is reflected in a decrease in intensity (*35*, *36*, *51*−*54*).

The Hb species whose 229 nm UVRR spectra exhibit a general decrease in the relative intensity of both tyrosine and

tryptophan bands are derivatives that are likely to be transition state species or resemble transition state species. These include the following R state species: deoxyHbs stabilized in the R structure (deoxy desHis/desTyr) (*35*), transient intermediates appearing within several hundred nanoseconds of photodissociating R state liganded HbA (*37*), and half-liganded Fe−Co hybrids stabilized in the R structure (*37*, *44*). Similarly, T state species that manifest the T state UVRR markers but with an across-the-board decrease in band intensities include liganded T state HbA trapped using sol−gel encapsulation techniques (*51*) and asymmetric ferrous−ferric(cyanomet) hybrids of HbA (*54*). On the basis of these observations, it is probable that the pattern of an overall intensity decrease in the 229 nm-excited UVRR spectrum (Figure 4) is indicative of a general loosening of those interactions responsible for stabilizing the respective quaternary state, as would be anticipated for a conformation approaching a transition state reaction coordinate.

Impact of Cys β93 Sulfhydryl Modification on COHb Derivatives. Earlier studies have shown that the liganded derivative of maleimide-modified HbA has both functional and spectroscopic properties that are altered (*16*, *17*, *21*, *22*, *24*). Most probes clearly indicate that the overall properties are consistent with the modified species adopting the R quaternary state when fully liganded. However, several parameters indicate a deviation from the behavior of R state HbA. Functionally, the modified liganded HbAs exhibit a reduced K_4, the equilibrium binding constant for the fourth ligand, indicating a reduced ligand binding affinity for the R state form of these derivatives (*22*). Consistent with this observation is our recent finding (*55*) that the geminate yield for the CO derivatives of the β93-modified species is reduced relative to that of COHbA, but with no obvious change in the R state bimolecular recombination from the solvent. It was also observed that the frequency of ν(Fe−His), the iron−proximal histidine stretching mode, is reduced for the 8 ns photoproducts of the CO derivatives of the β93-modified HbAs. A reduction in the iron−histidine stretching frequency correlates with a reduction in the geminate yield and indicates a reduction in the quaternary enhancement effect, i.e., the enhanced ligand binding of the R state tetramer relative to the separated dimers (*53*).

In the study presented here, most UVRR spectral features reflective of the hinge region (Trp β37−W3), the switch region (Tyr α42−Y8a), and the α-chain terminus (Tyr α140−Y8a) exhibit no readily identifiable changes in the standard liganded R state markers. The sole exception to this rule is a 1560 cm^{-1} W3 band that is found in the T − R difference spectra of NESHb (Figure 2) and $\beta\beta$-SP-P2K-Hb (Figure 6). This difference results from a slight upshift in the W3 peak of the ligated Hb species, and suggests a shift of at least one of the A helices (probably from the modified β-chains), resulting in a slight change in the $C_\alpha-C_\beta$ dihedral angle of the indole ring for either A helix Trp (*45*, *46*).

The UVRR data do not unambiguously account for the origin of the altered R state properties of β93-modified HbA; however, the data do provide some boundaries with which to explore the behavior of these Hbs. The UVRR data suggest that the functional alterations of the R state do not arise from changes in the hinge region of the $\alpha_1\beta_2$ interface, the switch region of the $\alpha_1\beta_2$ interface, or the α-chain terminus. Instead, the data are consistent with explanations based on the recently proposed (*55*) mechanism related to an induced shifting of the phenol side chain of Tyr β145 from its usual R state cleft. [It should be noted that Tyr β145 does not appear to contribute to the T versus R changes observed for Y8a (*49*, *50*).]

The shifting of the β145 phenol group out of the usual R state cleft can be the basis for altered reactivity through any of several "domino effect" mechanisms that do not directly perturb the $\alpha_1\beta_2$ interface. The β145 phenol group hydrogen bonds to the carbonyl of Val β98 in the FG corner. Disruption of this hydrogen bond could alter the positioning of the F helix and thus lead to the altered ν(Fe−His). The link to the altered function would follow from the correlation between the frequency of ν(Fe−His) for the early time photoproduct of COHb derivatives and the geminate yield. This mechanism is discussed in more detail in ref *55*.

Another possible β145-linked origin for the altered R state functionality could arise from either a static or a dynamic (temperature factors) perturbation of the surrounding helices (possibly through the disruption of the hydrogen bond to Val β98) that allows for a more rapid escape of dissociated ligand from the distal heme pocket. We have observed that the relaxation of the local tertiary structure associated with the heme pocket (including the proximal histidine) after photodissociation in various mutant COMbs is strongly coupled to the escape of the CO from the distal pocket into nearby hydrophobic cavities (unpublished results). Furthermore, it appears that this relaxation makes it more likely for a ligand returning to the distal pocket from a nearby hydrophobic cavity to escape into the solvent rather than rebind. Thus, a possible scenario for the β93-modified COHbAs is that the β93 modification alters β145 that, in turn, results in local alterations in the helical packing in the β-heme environment, leading to rapid escape of the dissociated ligand from the distal heme pocket. The rapid movement of the ligand from the distal pocket to adjacent cavities allows for an enhanced relaxation of the local tertiary structure, yielding the lower-frequency ν(Fe−His). The relaxed local tertiary structure, as reflected in ν(Fe−His), would then result in a higher kinetic barrier for the heme rebinding of any ligand returning to the distal heme pocket, and thus favor escape into the solvent. This model is currently being tested.

Impact of Cys β93 Sulfhydryl Modification on DeoxyHb Derivatives. The deoxy derivative of NEM-modified HbA exhibits increased ligand binding reactivity and spectroscopic features consistent with a destabilized T state species (*55*). These properties are ascribed to the disruption of the hydrogen bonding between Asp β94 and His β146 and between Lys α40 and His β146. Both of these hydrogen bonds have been shown to contribute to the stability of the deoxy T state (*56*, *57*). In the study presented here, all the deoxy derivatives of the β93-modified species, except for NESdes-Arg HbA, exhibit features that indicate that the hinge region of the $\alpha_1\beta_2$ interface remains T-like. The Y8a band of deoxyNESHbA, however, is broadened to a degree where it overlaps the corresponding Y8a bands of both deoxyHbA and COHbA. Given the proximity of Asp β94 to Asp β99, it is reasonable to tentatively attribute the broadening of Y8a to a weakening of the switch region Asp β99−Tyr α42 hydrogen bond. Tritium exchange results indicate that a solution of deoxyNESHbA is not a mixture of T and R state

species (*56*). Thus, the UVRR results suggest that the NES modification creates a deoxy species that retains the overall T state quaternary structure but with a "loosened" switch region. This conclusion is supported by recent experiments (*55*) in which sol−gel encapsulation techniques were used to trap and kinetically characterize CO-bound forms of NESHbA having the equilibrium T or R quaternary structure. The kinetic pattern for the nonequilibrium CO derivative of deoxyNESHbA locked in the T state quaternary conformation indicates that there is no mixing of the R and T states, only a liganded T state conformation having a higher yield of geminate recombination than a comparable liganded T state sample derived from encapsulated deoxyHbA. Similar conclusions can be applied to the maleimide-linked PEG HbA derivatives that have the phenyl carbamyl linkers (Figures 8a and 9). This group of derivatives also shows the broadened Y8a band. In contrast, both the PEG derivatives with non-phenyl linkers and the non-maleimide-modified GSSHbA (Figures 5, 8b, and 9) exhibit deoxy Hb Y8a bands that are shifted but not broadened with respect to the CO derivatives. Thus, it would appear that for these modified Hbs, the deoxy derivatives have a more "normal", i.e., wild-type, $\alpha_1\beta_2$ T state interface than NESHbA and the PEG derivatives having a phenyl carbamyl linker.

The combination of the NES and the des-Arg modification to HbA is known to produce a noncooperative, high-affinity species. The deoxy derivative exhibits a ν(Fe−His) frequency that is consistent with an R state species (*26*). The UVRR spectra reveal features that are very similar to those observed for deoxy derivatives retaining an R quaternary structure, e.g., desHis, desTyrHbA (*35*), and partially relaxed, photodissociated COHbA (*37*). The key spectroscopic indicators of the deoxy R state are peaks that are unshifted with respect to those from liganded R state species but with an overall decrease in intensity of most of the Raman bands as is reported herein for deoxyNESdes-ArgHbA (Figure 4).

Influence of PEG. Most of the features seen in the UVRR spectra of the maleimide-phenyl carbamyl-linked, PEG-decorated Hbs are very similar to those seen for NESHbA. The main distinctive feature common to all these materials is the broadened Y8a band for the deoxy derivatives. On the other hand, ethyl-linked PEG Hbs exhibit a general and substantial enhancement in the intensity of most UVRR bands (Table 1), and Y8a frequency shifts associated with the T to R state transition but no Y8a broadening. Again, the difference in signal enhancement between the phenyl- and ethyl-linked Hbs cannot be attributed to self-absorption by the phenyl groups because the laser is configured for front surface scattering off the sample. Global intensity changes in Trp and Tyr UVRR bands may result from variations in both the overall tightness of the packing of helices and the degree of surface hydration (*35*, *50*, *53*, *54*). The PEG-induced increase in band intensity shown here is consistent with PEG causing either a compaction of the overall structure and/or a decrease in the water content of the Hb molecule. Of course, if the effect of PEG is to partially dehydrate the protein, then a compaction of structure can result. The observation that the linker group plays a determining role for this effect suggests that the spacing between the PEG and the surface of the protein is critical or that there is a linker-dependent sensitization of the globin to the presence of the PEG. It is possible that with the non-phenyl maleimide linkers, the PEG is sufficiently close to the surface of the protein to exert an effective osmotic stress on the protein in much the same way that glycerol does. With the longer phenyl carbamyl linker, there might be adequate spacing between the PEG and the surface of the protein to maintain a full solvation shell of water. The effect of PEG on HbA hydration under solution conditions is difficult to assess since a buffer solution containing >50% (w/w) PEG6000 resulted in precipitation of COHbA (U. Samuni, unpublished results). However, deoxyHbA and COHbA may be encapsulated in a sol−gel matrix that remains porous to buffer solution. For encapsulated HbA, the effect of a 50% (w/w) PEG6000 buffer solution [50 mM Bis Tris acetate (pH 6.5)] on UVRR W3 and Y8a peak intensities varied with ligation state (data not shown). For encapsulated COHbA, the presence of PEG6000 resulted in a 0.11 increase in the intensity of the W3 β37 band only, whereas both the W3 and Y8a band intensities increased ($\Delta W3_{\alpha 14/\beta 15} = 0.19$, $\Delta W3_{\beta 37} = 0.43$, and $\Delta Y8a = 0.24$) for encapsulated deoxyHbA. These results support the general idea that PEG affects the HbA hydration shell.

CONCLUSION

The major effect of β93 modification is a disruption of the T state Tyr α42−Asp β99 hydrogen bond in the switch region of the $\alpha_1\beta_2$ interface as revealed by the Y8a UVRR band for deoxy derivatives of phenyl carbamyl-linked Hbs. These broadened Y8a bands suggest either the presence of a mix of both T and R state interactions or a PEG-induced osmotic stress on the switch region of the T state $\alpha_1\beta_2$ interface. This region undergoes a large redistribution of water molecules with a change in quaternary structure; hence, it is reasonable that attached PEG groups could exert an observable osmotic effect on this domain.

The UVRR spectra of the β93-modified COHbs show no evidence of a destabilization of the R state interfacial interactions, suggested by reductions in both the geminate yield and the frequency of the iron−proximal histidine stretching mode for the R state photoproduct (*55*). The UVRR results are consistent with the idea that these R state effects arise from local changes in the packing of Tyr β145 (*55*).

For deoxy and CO derivatives of β93-modified Hbs with ethyl maleimide-linked PEG, the UVRR spectra indicate that the PEG is capable of inducing a general "tightening" or compaction of the global structure. This effect is likely to originate from the osmotic consequences of having large and/or numerous PEG chains on the surface of the protein. The effect is highly dependent on the nature of the linker group joining the PEG to the maleimide. The results suggest that the linker mediates the effect either by controlling the separation between the PEG and the surface of the protein or by sensitizing the local surface domain, rendering it vulnerable to the osmotic impact of the PEG. In either case, our study indicates that PEG-induced effects on proteins may be able to be tuned via a suitable choice of a linker group.

Surface decoration of HbA with PEG chains is actively being explored as a means of generating size-enhanced, acellular Hb-based, oxygen transport reagents. This study indicates that specific PEG-based reagents can be used to achieve size-enhanced Hbs with minimal perturbation of

either the R or T state quaternary conformations, as is especially evident for $(SP\text{-}P5K)_6$-HbA. This finding stands in contrast to the highly altered properties associated with many of the commercial products that utilize polymerization to achieve size-enhanced Hbs.

REFERENCES

1. Dickerson, R. E., and Geis, I. (1983) *Hemoglobin: Structure, Function, Evolution, and Pathology*, Benjamin/Cummings Publishing Co., Menlo Park, CA.
2. Antonini, E., and Brunori, M. (1971) *Hemoglobins and Myoglobins in their Reactions with Ligands*, Elsevier, New York.
3. Jia, L., Bonaventura, C., Bonaventura, J., and Stamler, J. S. (1996) *Nature 380*, 221−226.
4. Stamler, J. S., Jia, L., Eu, J. P., McMahon, T. J., Demchenko, I. T., Bonaventura, J., Gernert, K., and Piantadosi, C. A. (1997) *Science 276*, 2034−2037.
5. Balagopalakrishna, C., Abugo, O. O., Horsky, J., Manoharan, P. T., Nagababu, E., and Rifkind, J. M. (1998) *Biochemistry 37*, 13194−13202.
6. Manjula, B. N., Malavalli, A., Smith, P. K., Chan, N. L., Arnone, A., Friedman, J. M., and Acharya, A. S. (2000) *J. Biol. Chem. 275*, 5527−5534.
7. Craescu, C. T., Poyart, C., Schaeffer, C., Garel, M. C., Kister, J., and Beuzard, Y. (1986) *J. Biol. Chem. 261*, 14710−14716.
8. Garel, M. C., Domenget, C., Caburi-Martin, J., Prehu, C., Galacteros, F., and Beuzard, Y. (1986) *J. Biol. Chem. 261*, 14704−14709.
9. Perutz, M. F., Fermi, G., Luisi, B., Shaanan, B., and Liddington, R. C. (1987) *Acc. Chem. Res. 20*, 309−321.
10. Perutz, M. F., Wilkinson, A. J., Paoli, M., and Dodson, G. G. (1998) *Annu. Rev. Biophys. Biomol. Struct. 27*, 1−34.
11. Perutz, M. F. (1970) *Nature 228*, 726−739.
12. Guidotti, G. (1965) *J. Biol. Chem. 240*, 3924−3927.
13. Guidotti, G. (1967) *J. Biol. Chem. 242*, 3704−3712.
14. Taketa, F., and Morell, S. A. (1969) *Anal. Biochem. 32*, 169−174.
15. Vasquez, G. B., Karavitis, M., Ji, X., Pechik, I., Brinigar, W. S., Gilliland, G. L., and Fronticelli, C. (1999) *Biophys. J. 76*, 88−97.
16. Perutz, M., Ladner, J., Simom, S., and Ho, C. (1974) *Biochemistry 13*, 2163−2173.
17. Perutz, M. F., Fersht, A. R., Simon, S. R., and Roberts, G. C. (1974) *Biochemistry 13*, 2174−2186.
18. Perutz, M. F., Heidner, E. J., Ladner, J. E., Beetlestone, J. G., Ho, C., and Slade, E. F. (1974) *Biochemistry 13*, 2187−2200.
19. Doyle, M. L., and Ackers, G. K. (1992) *Biochemistry 31*, 11182−11195.
20. Doyle, M. L., Lew, G., Turner, G. J., Rucknagel, D., and Ackers, G. K. (1992) *Proteins 14*, 351−362.
21. Kilmartin, J. V., Hewitt, J. A., and Wootton, J. F. (1975) *J. Mol. Biol. 93*, 203−218.
22. Imai, K. (1973) *Biochemistry 12*, 798−808.
23. Imai, K. (1973) *Biochemistry 12*, 128−134.
24. Riggs, A. F. (1961) *J. Biol. Chem. 236*, 1948−1954.
25. Taketa, F., Chen, J. Y., Skogen, W. F., Litwin, S. B., and Laver, M. B. (1978) *Hemoglobin 2*, 261−273.
26. Ondrias, M. R., Rousseau, D. L., Shelnutt, J. A., and Simon, S. R. (1982) *Biochemistry 21*, 3428−3437.
27. Asher, S. (1993) *Anal. Chem. 65*, 59A−66A.
28. Austin, J., Jordan, T., and Spiro, T. (1993) in *Biomolecular Spectroscopy, Part A* (Clark, R. J. H., and Hester, R. E., Eds.) pp 55−127, John Wiley and Sons, New York.
29. Kitagawa, T. (1992) *Prog. Biophys. Mol. Biol. 58*, 1−18.
30. Su, C., Park, Y. D., Liu, G., and Spiro, T. G. (1989) *J. Am. Chem. Soc. 111*, 3457−3459.
31. Rodgers, K., Su, S., Subramaniam, S., and Spiro, T. (1992) *J. Am. Chem. Soc. 114*, 3697−3709.
32. Jayaraman, V., Rodgers, K. R., Mukerji, I., and Spiro, T. G. (1993) *Biochemistry 32*, 4547−4551.
33. Jayaraman, V., Rodgers, K. R., Mukerji, I., and Spiro, T. G. (1995) *Science 269*, 1843−1848.
34. Nagai, M., Kaminaka, S., Ohba, Y., Nagai, Y., Mizutani, Y., and Kitagawa, T. (1995) *J. Biol. Chem. 270*, 1636−1642.
35. Wang, D., and Spiro, T. G. (1998) *Biochemistry 37*, 9940−9951.
36. Wang, D., Zhao, X., Shen, T. S., Ho, C., and Spiro, T. G. (1999) *J. Am. Chem. Soc. 121*, 11197−11203.
37. Rodgers, K. R., and Spiro, T. G. (1994) *Science 265*, 1697−1699.
38. Hu, X., and Spiro, T. G. (1997) *Biochemistry 36*, 15701−15712.
39. Hu, X. H., Rodgers, K. R., Mukerji, I., and Spiro, T. G. (1999) *Biochemistry 38*, 3462−3467.
40. Huang, S., Peterson, E. S., Ho, C., and Friedman, J. M. (1997) *Biochemistry 36*, 6197−6206.
41. Acharya, A. S., and Sussman, L. G. (1983) *J. Biol. Chem. 258*, 13761−13767.
42. Ampulski, R. S., Ayers, V. E., and Morell, S. A. (1969) *Anal. Biochem. 32*, 163−169.
43. Juszczak, L., Hirsch, R., Nagel, R., and Friedman, J. (1998) *J. Raman Spectrosc. 29*, 963−968.
44. Mukerji, I., and Spiro, T. G. (1994) *Biochemistry 33*, 13132−13139.
45. Maruyama, T., and Takeuchi, H. (1995) *J. Raman Spectrosc. 26*, 319−324.
46. Miura, T., Takeuchi, H., and Harada, I. (1989) *J. Raman Spectrosc. 20*, 667−671.
47. Samuni, U., Navati, M. S., Juszczak, L. J., Dantsker, D., Yang, M., and Friedman, J. M. (2000) *J. Phys. Chem. B 104*, 10802−10813.
48. Zhao, X., Chen, R., Raj, V., and Spiro, T. G. (2001) *Biopolymers 62*, 158−162.
49. Nagai, M., Wajcman, H., Lahary, A., Nakatsukasa, T., Nagatomo, S., and Kitagawa, T. (1999) *Biochemistry 38*, 1243−1251.
50. Wang, D., Zhao, X., and Spiro, T. G. (2000) *J. Phys. Chem. A 104*, 4149−4152.
51. Juszczak, L., and Friedman, J. (1999) *J. Biol. Chem. 274*, 30357−30360.
52. Dick, L., Heibel, G., Moore, E., and Spiro, T. (1999) *Biochemistry 38*, 6406−6410.
53. Huang, J., Juszczak, L. J., Peterson, E. S., Shannon, C. F., Yang, M., Huang, S., Vidugiris, G. V., and Friedman, J. M. (1999) *Biochemistry 38*, 4514−4525.
54. Jayaraman, V., and Spiro, T. G. (1995) *Biochemistry 34*, 4511−4515.
55. Khan, I., Dantsker, D., Samuni, U., Friedman, A. J., Bonaventura, C., Manjula, B., Acharya, S. A., and Friedman, J. M. (2001) *Biochemistry 40*, 7581−7592.
56. Englander, J. J., Rumbley, J. N., and Englander, S. W. (1998) *J. Mol. Biol. 284*, 1707−1716.
57. Englander, J. J., Louie, G., McKinnie, R. E., and Englander, S. W. (1998) *J. Mol. Biol. 284*, 1695−1706.

BI011212R